ELSEVIER

International Journal of Heat and Fluid Flow 23 (2002) 750–757

International Journal of HEAT AND FLUID FLOW

www.elsevier.com/locate/ijhff

Reynolds averaged simulation of flow and heat transfer in ribbed ducts

A. Ooi [a,*], G. Iaccarino [b], P.A. Durbin [c], M. Behnia [d]

[a] Department of Mechanical and Manufacturing Engineering, University of Melbourne, Melbourne 3010, Australia
[b] Center for Turbulence Research, Stanford University, CA 94305-3030, USA
[c] Department of Mechanical Engineering, Stanford University, CA 94305-3030, USA
[d] School of Mechanical and Manufacturing Engineering, University of New South Wales, Sydney 2052, Australia

Accepted 14 April 2002

Abstract

The accuracy of modern eddy-viscosity type turbulence models in predicting turbulent flows and heat transfer in complex passages is investigated. The particular geometries of interest here are those related to turbine blade cooling systems. This paper presents numerical data from the calculation of the turbulent flow field and heat transfer in two-dimensional (2D) cavities and three-dimensional (3D) ribbed ducts. It is found that heat transfer predictions obtained using the v^2–f turbulence model for the 2D cavity are in good agreement with experimental data. However, there is only fair agreement with experimental data for the 3D ribbed duct. On the wall of the duct where ribs exist, predicted heat transfer agrees well with experimental data for all configurations (different streamwise rib spacing and the cavity depth) considered in this paper. But heat transfer predictions on the smooth-side wall do not concur with the experimental data. Evidence is provided that this is mainly due to the presence of strong secondary flow structures which might not be properly simulated with turbulence models based on eddy viscosity.

1. Introduction

Accurate evaluation of heat loads in the components of a gas-turbine engine is a key factor in the development of new, efficient engines. Common design techniques utilize experimental data correlations to quickly estimate the heat transfer coefficients (Webb et al., 1971). These methods do not reveal the underlying mechanism of turbulence and heat transfer for the device in question. They often are inaccurate. Owing to advances in available computer resources, elaborate numerical techniques, based on the solution of the full 3D Reynolds averaged Navier–Stokes (RANS) equations, are now being used to shed light on the flow phenomena and to provide guidelines to improve design methodology. In the RANS approach, the Navier–Stokes equations are averaged and the Reynolds stresses are computed with a turbulence model. The choice of turbulence model is crucial, as it directly affects the computational requirements and the accuracy of the predictions. In particular, because most of the gas turbine cooling systems promote turbulence close to the walls to enhance heat transfer, precise near-wall turbulence modeling is crucial to ensure accurate heat transfer predictions.

In this paper, the ability to predict heat transfer coefficients in ducts with artificial roughness elements (ribs) is investigated. To evaluate the accuracy of the predictions, numerical solutions are compared to the experimental data of Rau et al. (1998). This particular data set was chosen because both flow field and heat transfer data are available. Additional experimental data that can be used to assess the accuracy of the numerical predictions are available from Han et al. (1978, 1985), Chyu and Wu (1989), Hirota et al. (1992) and Liou et al. (1993b).

Numerical predictions of the flow and heat transfer in rib-roughened passages have been conducted previously by several investigators: Simoneau and Simon (1992) showed that the conventional k–ϵ turbulence model with wall functions does not accurately predict the heat transfer level, due to the presence of massive separation in the flow field; Stephens (1995) found that the k–ω

* Corresponding author.
E-mail address: a.ooi@unimelb.edu.au (A. Ooi).

0142-727X/02/$ - see front matter © 2002 Elsevier Science Inc. All rights reserved.
PII: S0142-727X(02)00188-1

model showed only reasonable qualitative agreement with experimental data; Liou et al. (1993a) obtained good agreement with experimental data (on the symmetry plane) in a 2D Navier–Stokes calculation with the k–ϵ–A algebraic stress and heat flux model—however, the application of this model to complex 3D problems is computationally expensive and the model is numerically stiff (Gatski and Speziale, 1993; Speziale, 1997). More recently, it has been shown by Iacovides (1998) that two-layer k–ϵ with the effective viscosity model gives unsatisfactory heat transfer predictions in rotating ribbed passages. Better results were obtained with the two-layer approach coupled to a low-*Re* differential stress model. Computations with low-*Re* models were carried out by Iacovides and Raisee (1999), who found that improved heat transfer predictions could be obtained by introducing a differential version of the Yap length scale correction term which is independent of the wall distance.

Here, we revisit the ribbed duct problem. Since it has been shown that simplified wall treatments (wall functions, two layer, etc.) or methods that use empirical correlations (low-*Re* models) cannot correctly capture the separation and reattachment that takes place between successive ribs, we will examine the predictive capability of two more recent turbulence models: v^2–f and Spalart–Allmaras (S–A).

The v^2–f turbulence model was developed around the elliptic relaxation method for representing near-wall phenomena (Durbin and Pettersson-Reif, 2001). Unlike the low-*Re* approach, this is done without the aid of damping functions. It has been successfully applied to separated flow (Durbin, 1995), 3D boundary layers (Parneix et al., 1998) and impinging jets (Behnia et al., 1998, 1999). In the present work, v^2–f is used to predict flow and heat transfer in a 3D duct with ribs and in a model configuration resembling the tip of an axial turbine blade (Metzger et al., 1989).

Simulations have also been carried out with the S–A model. This is a one-equation, eddy-viscosity transport formulation, developed by Spalart and Allmaras (1992) and has proven to be both robust and accurate in aerodynamic applications (Bardina et al., 1997). Its accuracy for predicting internal flows has been largely untested, but is now addressed in this paper and in Kalitzin and Iaccarino (1999) (see also Durbin and Pettersson-Reif, 2001). Results from the standard two-layer k–ϵ model (Chen and Patel, 1988) are also included here for comparison.

2. Numerical model

As there is separation in the flows under consideration, it is expected that wall functions will be unable to accurately reproduce the experimental data. Hence, only turbulence models that can be integrated all the way to the wall—two-layer k–ϵ, v^2–f and S–A—were used in the simulations. The governing equations for the v^2–f model are

$$\frac{\partial k}{\partial t} + U\nabla k = P_k - \epsilon + \nabla[(\nu + \nu_t)\nabla k], \tag{2.1}$$

$$\frac{\partial \epsilon}{\partial t} + U\nabla \epsilon = \frac{C_{\epsilon 1}P_k - C_{\epsilon 2}\epsilon}{T} + \nabla\left[\left(\nu + \frac{\nu_t}{\sigma_\epsilon}\right)\nabla\epsilon\right], \tag{2.2}$$

$$\frac{\partial v^2}{\partial t} + U\nabla v^2 = kf - nv^2\frac{k}{\epsilon} + \nabla[(\nu + \nu_t)\nabla v^2], \tag{2.3}$$

$$L^2\nabla^2 f - f = \frac{1}{T}\left[(C_1 - n)\frac{v^2}{k} - (C_1 - 1)\frac{2}{3}\right] - C_2\frac{P_k}{k}, \tag{2.4}$$

where

$$T = \max\left[\frac{k}{\epsilon}, 6\left(\frac{\nu}{\epsilon}\right)^{1/2}\right],$$

$$L = C_L \max\left[\frac{k^{3/2}}{\epsilon}, C_\eta\left(\frac{\nu^3}{\epsilon}\right)^{1/4}\right]. \tag{2.5}$$

P_k is the production of kinetic energy given by

$$P_k = 2\nu_t S_{ij} S_{ij}, \tag{2.6}$$

where ν_t is the eddy viscosity given by

$$\nu_t = C_\mu v^2 T. \tag{2.7}$$

n is either 1 or 6, the latter being a modification introduced to reduce stiffness when using a segregated solution scheme. The model constants for $n = 6$ are

$$\begin{aligned} &C_\mu = 0.22, \quad \sigma_\epsilon = 1.3, \\ &C_{\epsilon 1} = 1.4(1 + 0.045\sqrt{k/v^2}), \quad C_{\epsilon 2} = 1.9, \\ &C_1 = 1.4, \quad C_2 = 0.3, \quad C_L = 0.23, \quad C_\eta = 70. \end{aligned} \tag{2.8}$$

The formulations of the S–A and two-layer k–ϵ models can be found in Durbin and Pettersson-Reif (2001) and will not be repeated here.

The temperature field is computed with an eddy diffusivity approximation for the turbulent heat flux. Values of Pr_t used in the literature vary from 0.73 to 0.92. In this paper, a constant value of $Pr_t = 0.85$ was used for all the computations. This value was considered by Kays (1994) to be generally acceptable.

All governing equations are discretized by a second order upwind-biased scheme; all quantities at the cell faces are calculated using a multidimensional linear reconstruction approach (Barth and Jesperson, 1989) and then solved in a segregated manner.

A commercial computational fluid dynamics (CFD) software, FLUENT 5.5, was used to solve the equations. The SIMPLE (semi-implicit method for pressure-linked equations) algorithm was selected for the incompressible flow computation. The two-layer k–ϵ and the S–A

models are those that exist in FLUENT 5.5. The v^2–f model was coded separately as a subroutine and was incorporated into the CFD code. The implementations of all models have been validated against previously published results in the open literature.

3. Geometry and grid

Two configurations are considered in this paper. The ribbed duct simulations are carried out using a 3D grid with periodic boundary conditions in the streamwise, X, direction and symmetry is assumed at the mid-duct plane. Ribs of height e (see Fig. 1) are placed either on one wall (1s) or on two opposite walls (2s). For the 1s simulations, the no-slip condition is applied on the top wall ($Y/e = 10$) and symmetry is invoked at the mid-duct ($Z/e = 5$). For the 2s simulations, symmetry is imposed on the top ($Y/e = 5$) and at the mid-duct ($Z/e = 5$); thus, only one quarter of the domain need be computed. In both situations, the flow is assumed to be fully developed; hence, periodic conditions are applied in the streamwise direction. The rib height-to-duct hydraulic diameter ratio is $e/D_h = 0.1$, so the blockage ratio of the ribs is 10% or 20% for cases 1s and 2s, respectively. The duct width-to-height ratio (W/H) is unity and the pitch to rib-height ratios, p/e, are 6, 9 and 12. The Reynolds number, Re, is 30,000 based on D_h and the bulk velocity, U_b. The fluid Prandtl number for all calculations is 0.71.

Grids used consist of ≈180,000 ($p/e = 9$ and 2s), 250,000 ($p/e = 6$ and 1s), 300,000 ($p/e = 9$ and 1s) and 360,000 ($p/e = 12$ and 1s) hexahedral elements. Since only turbulence models that can be integrated to the surface will be used, all grids have strong clustering close to the walls to ensure that the first computational node is at $y^+ \approx 1$. To ensure that all results reported here are grid independent and well resolved, all simulations were repeated with twice the number of grid points in each spatial direction. No noticeable difference in the solutions were observed.

The second configuration investigated in this paper is a schematic of the grooved tip cross-section of a turbine blade. The ratio of clearance height to cavity width, c/w, was fixed at 0.1 and two different cavity depths are considered, corresponding to d/w of 0.1 and 0.2 (see Fig. 10 for an illustrative definition of c, w and d). The experimental investigation carried out by Metzger et al. (1989) was at a Reynolds number based on the bulk velocity and the clearance, c, of 15,000. The computational grid consists of ≈20,000 elements, with clustering at the walls to correctly capture the flow features in the viscous layers.

4. Results and discussion

4.1. The ribbed duct

Fig. 1 shows the flow pattern on the symmetry plane for $p/e = 12$, computed with the k–ϵ model. All other turbulence models produce a similar flow pattern. The conventional flow pattern exists: the flow separates after going over the upstream rib, creating a low pressure region behind the rib. There is a primary recirculation bubble, with a small secondary recirculation region directly after the upstream rib. Further downstream, the flow reattaches and forms a short recovery region. This flow then impinges on the next rib, forming a small recirculating region in front of it. With $p/e = 6$ the same recirculation regions exist. However, all computations for $p/e = 6$ (not shown here) show that on the symmetry plane, the main recirculation bubble does not reattach.

The lateral variation of the separation region can be investigated by plotting the streamwise velocity, U/U_b, on a plane that is very close to the floor of the duct. Fig.

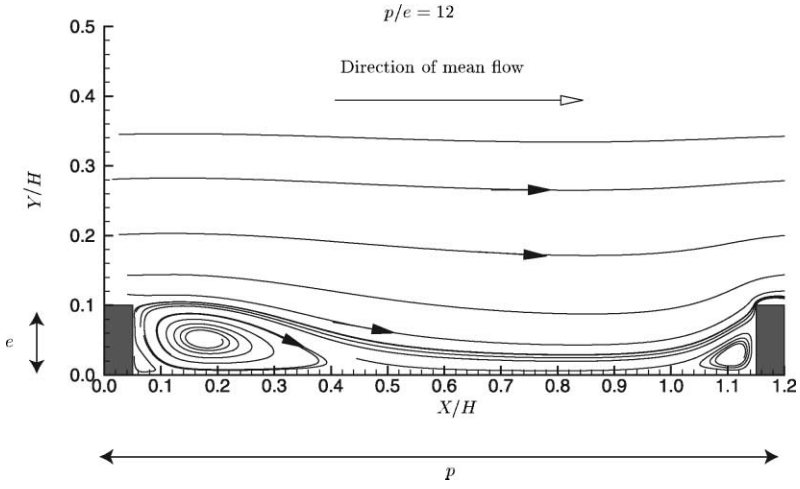

Fig. 1. Mean streamlines on the symmetry plane for the ribbed passage: $Re = 30{,}000$.

2 shows a plot of the streamwise velocity on a plane right above the floor ($Y/e = 0.1$) for both $p/e = 6$ and $p/e = 12$ (all models show qualitatively this result). It is clear from Fig. 2(a) that for $p/e = 6$, the primary recirculation bubble does not reattach onto the floor between the two ribs. This is in contrast with the experimental data of Rau et al. (1998) who found that the flow reattaches to the side wall at $\approx Z/e = 1$, even though it remains separated on the symmetry plane. The results for $p/e = 12$, in Fig. 2(b), indicate a reattachment point close to the symmetry plane. As we get closer to the wall, at Z/e around 0.5, there is no clear region where the flow reattaches.

Fig. 3 shows the spatial variation of the Y component of velocity, V/U_b, on the symmetry plane along the height of the rib ($Y/e = 1$) in between the two ribs. The 1s simulation with $p/e = 12$ is shown. Data in this figure illustrate the strength of the entrainment of cold mainstream fluid. This vertical motion in the separated region behind the rib leads to a secondary flow that drives the mainstream fluid toward the smooth-side wall (Rau et al., 1998). It is clear from this figure that all models underpredict the magnitude (strength) of this downward vertical motion. This in turn leads to an underprediction of the strength of the impingement which then leads to underprediction of heat transfer from the floor between the two ribs (see Fig. 6).

The mean secondary flow structure which exists in the 2s and $p/e = 9$ S–A simulations is shown in Fig. 4(a).

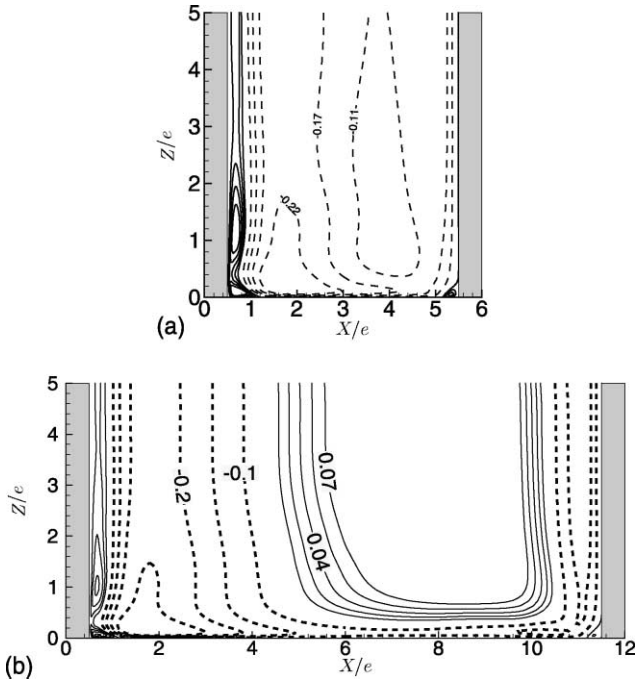

Fig. 2. Contour plots of the streamwise velocity profile for $p/e = 6$ (a) and $p/e = 12$ (b) on $y/e = 0.1$. Solid contour lines indicate positive values of U and negative values of U are represented by dashed contour lines. $Re = 30{,}000$.

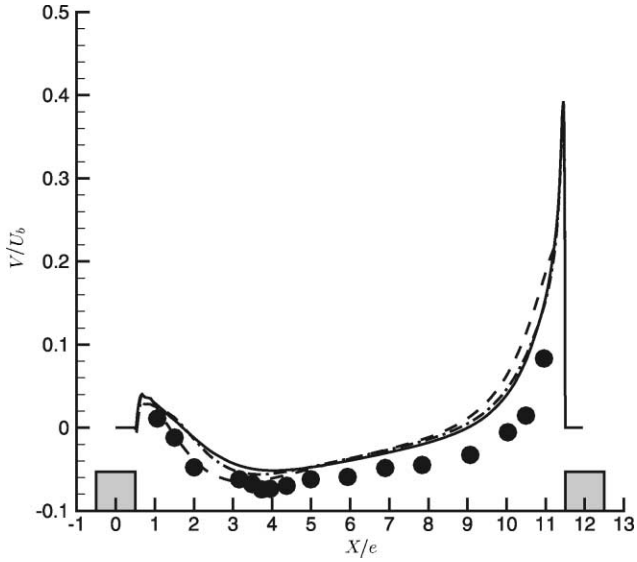

Fig. 3. Predicted and experimental V velocity profiles at $Y/e = 1.0$ for $p/e = 12$ on the symmetry plane at $Re = 30{,}000$. (●) Rau et al. (1998), (- - - -) k–ϵ, (– · –) S–A, (—) v^2–f.

These spanwise structures have been experimentally studied by Liou et al. (1993b) using LDV techniques. A qualitative sketch of their results is included in Fig. 4(b). It is clear in the experimental data that one secondary flow cell exists in each quadrant of the duct cross-section. The center of this secondary flow is toward the side wall and it is believed that the 'impinging effect' of this secondary structure (on the side wall) is responsible for the high heat transfer rates from the side wall. No such structure exists in the simulation, which could explain the large discrepancy between the predicted and experimentally measured heat transfer on the side wall—seen later.

In the heat transfer predictions, all Nusselt number distributions for the ribbed duct calculations presented here will be normalized by the level obtained in a smooth circular tube (Rau et al., 1998):

$$Nu_0 = 0.023 Re^{0.8} Pr^{0.4}. \tag{4.1}$$

Contours of Nu/Nu_0 for $p/e = 12$, computed using the k–ϵ model, are shown in Fig. 5. Results from all other models are alike. Qualitatively, the contours are similar to the experimental data of Rau et al. (1998). On the side wall, maximum values of Nu appear on the top of the upstream rib and on the first corner of the downstream rib. The value of Nu decreases until $Y/e \approx 6$ and then increases again as the top wall is approached. On the floor between the two ribs, maximum heat transfer occurs on the symmetry plane, in the vicinity of the reattachment point of the primary recirculating bubble. Even though the qualitative observations agree with the experimental results of Rau et al. (1998), the quantitative values of Nu/Nu_0 differ significantly from the experimental values. The highest contour level reported in

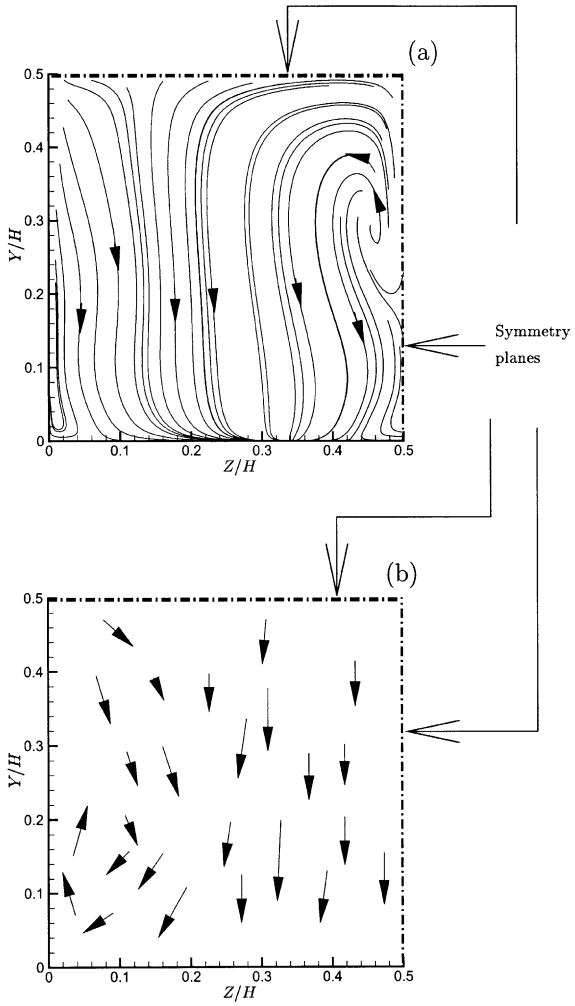

Fig. 4. Spanwise flow structure for the 2s, $p/e = 9$ simulation at the plane in between the two ribs ($X/e = 4.5$): (a) the prediction using the Spalart–Allmaras model and (b) a sketch of the vectors obtained by Liou et al. (1993b). $Re = 30{,}000$.

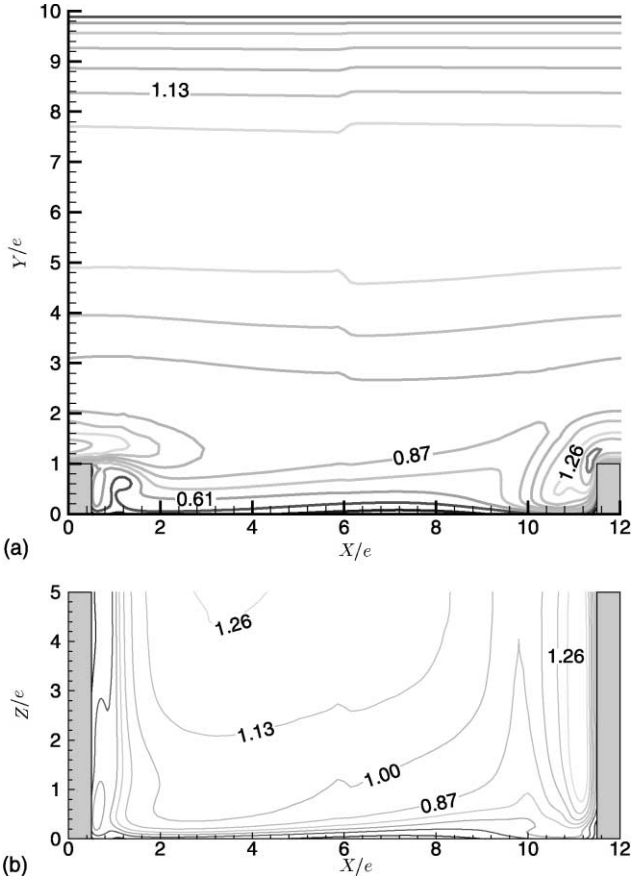

Fig. 5. Contours of Nu/Nu_0 on the side wall (a) and on the floor of the duct (b): $Re = 30{,}000$, $Pr = 0.71$.

Rau et al. (1998) was 2.24 which is nearly twice the value of 1.26 shown in Fig. 5(a). This is due to the under-prediction of secondary flow motion, as discussed previously.

On the bottom wall between the two ribs, contours of Nu/Nu_0 show two local maxima as can be seen in Fig. 5(b). One local maximum is located close to the reattachment point of the primary recirculation bubble. The other local maximum occurs just upstream of the downstream rib. For lower values of p/e only one local maximum of Nu is observed in the numerical data. This is qualitatively similar to the results of Rau et al. (1998) but the magnitude of Nu is again significantly smaller than the experimental values.

Heat transfer predictions for the one sided ribbed duct with $p/e = 9$ using all models are shown in Fig. 6. The variation of Nu in the streamwise direction on the symmetry plane is plotted. The heat transfer predicted by the k–ϵ model is roughly half the heat transfer measured in the experiment for both the configurations analyzed. Calculations reported in the literature (Iaco-

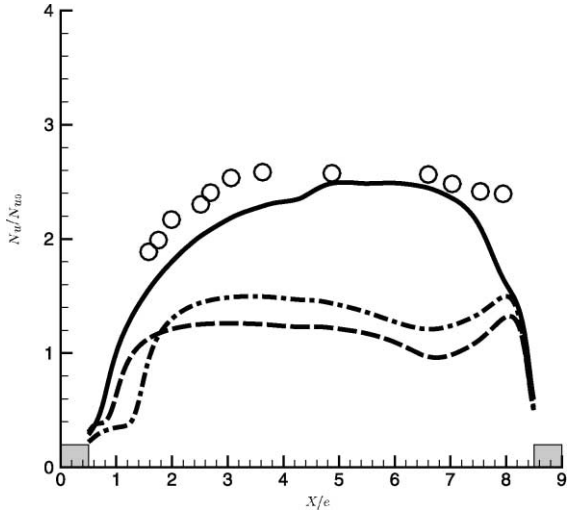

Fig. 6. Comparing the heat transfer predictions using various turbulence models with experimental data for $p/e = 9$ and 1s configuration. (◯) Rau et al. (1998), (----) k–ϵ, (–·–) S–A, (—) v^2–f. $Re = 30{,}000$, $Pr = 0.71$.

vides, 1998) using the same k–ϵ model and different p/e and e/D_h ratios also show the same quantitative disagreement. The S–A model produces a slightly better agreement but the quantitative value is still well below the values reported in the experiment. For all cases tested here, with various p/e values, the v^2–f model gave heat transfer predictions that are closest to the experimental measurements. It has been observed from experimental data that the rate of heat transfer decreases as the p/e ratio is increased from 9 to 12. The v^2–f (Fig. 7) model reproduces this trend.

Fig. 8 compares the predicted values of Nu on the side wall to experimental data. The comparison is taken a distance e from the center of the downstream rib. It is clear that all models make relatively bad predictions on the side wall. They all underpredict the value of Nu close to the floor. This is clearly due to the absence of the 'impinging effect', owing to an inability to reproduce the secondary motion in the duct—as discussed above. Closer to the top wall, the value of Nu is underpredicted by k–ϵ and overpredicted by both S–A and v^2–f.

In terms of averaged heat transfer (Nu_{ave}) on the floor between the two ribs, reported data in Fig. 9, the v^2–f predictions are closer to the experimental values than the two other models. However, the level of Nu is again underpredicted. Looking at the data in Fig. 6, one would expect that the averaged level of Nu to be closer to the experimental data than the values shown in Fig. 9, especially for the case where $p/e = 9$. However, the results in Fig. 6 only show the predictions on the symmetry plane of the ribbed duct: predictions get progressively worse as one moves away from the symmetry plane, towards the smooth-side wall. The predicted average value of Nu on the smooth wall is shown in Fig. 9(b).

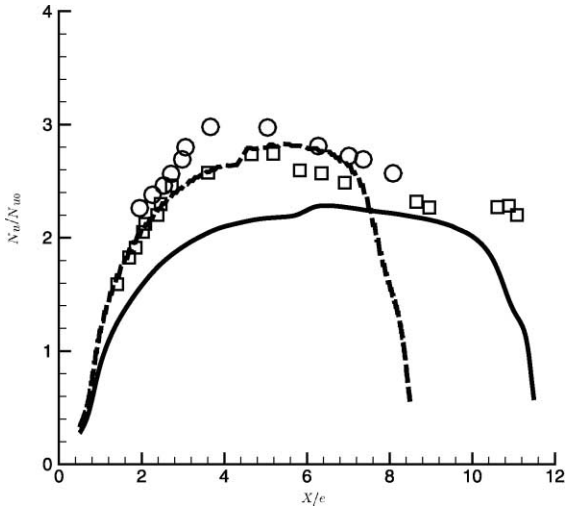

Fig. 7. Comparing the predictions using v^2–f model with experimental data for different geometrical configurations. Data for $p/e = 9$ and 2s are denoted by (◯) Rau et al. (1998) and (- - - -) v^2–f model prediction. Data for $p/e = 12$ and 1s are denoted by (□) Rau et al. (1998) and (—) v^2–f model prediction. $Re = 30{,}000$, $Pr = 0.71$.

In light of Fig. 8, it is surprising that the average value of Nu predicted by the models on the side wall

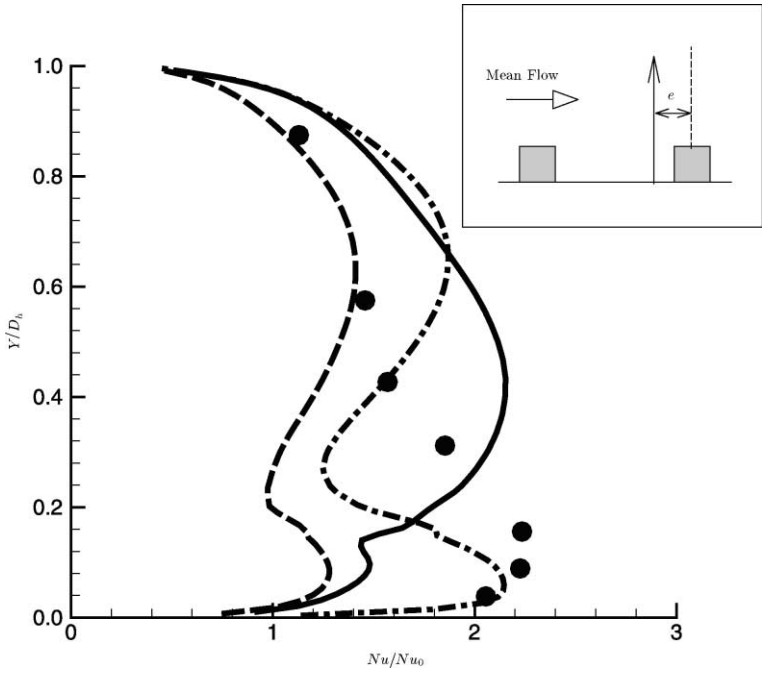

Fig. 8. Comparing the Nu predictions on the side wall with different turbulence models. Comparison data taken on the side wall, distance e from the downstream rib for the case with 1s and $p/e = 9$. (●) Rau et al. (1998), (- - - -) k–ϵ, (–·–) S–A, (—) v^2–f. $Re = 30{,}000$, $Pr = 0.71$.

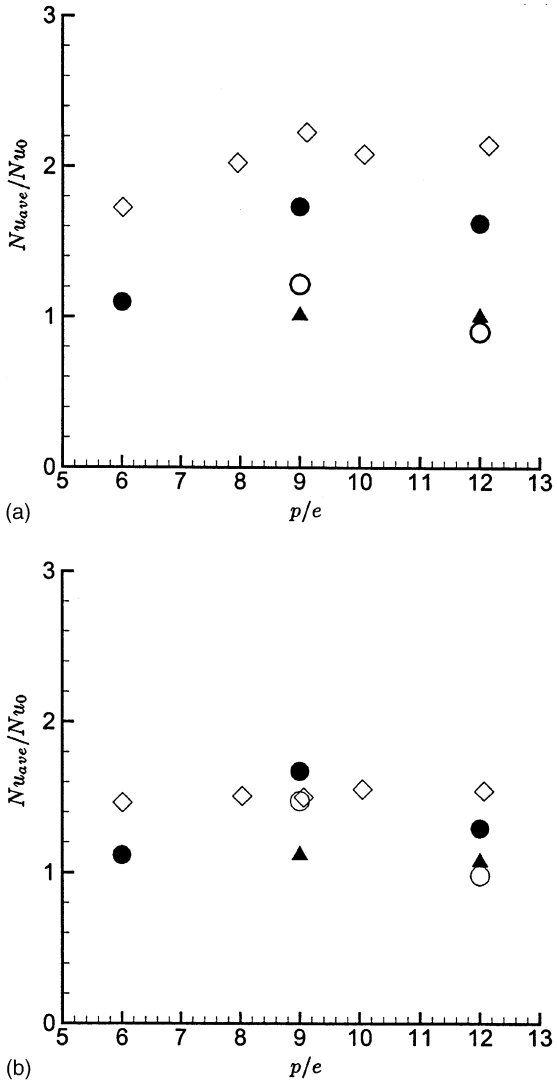

Fig. 9. Averaged Nusselt number for the ribbed passage. Bottom wall between ribs (a) and smooth-side wall (b). (◇) Rau et al. (1998), (▲) k–ϵ, (◯) S–A, (●) v^2–f. $Re = 30{,}000$, $Pr = 0.71$.

agree quite well with the experimental values. This is due to the fact that both the v^2–f and the S–A models *underpredict Nu* closer to the floor and *overpredict Nu* as the top wall is approached. This under and overprediction of *Nu* results in an average value of *Nu* that by coincidence agree quite well with the experimental data.

4.2. The 2D cavity

Computed streamline patterns for the flow in the cavity with $d/w = 0.2$ are shown in Fig. 10. The flow separates as it leaves the upstream corner and reattaches on the vertical wall downstream. A slow recirculating region develops in the cavity and the flow pattern resembles a driven cavity flow. For $d/w = 0.1$, the flow pattern (which is not shown here) is very similar to that of Fig. 1. The flow separates at the upstream corner and reattaches on the floor.

Heat transfer predictions on the floor between the two walls are found in Fig. 11. As in the case of the ribbed duct, the Nusselt number predicted by the k–ϵ model is too low. On the other hand, v^2–f gives good agreement with experimental data. The agreement with experimental data is better for the flow with $d/w = 0.2$ (Fig. 11(b)) than $d/w = 0.1$ (Fig. 11(a)). It is interesting to note that the experimental data with $d/w = 0.1$ show a peak in the Nusselt number close to downstream wall. The v^2–f model reproduces this peak whereas the k–ϵ model predicts a dip in the heat transfer.

5. Conclusions

Simulation of the flow and heat transfer in rib-roughened ducts and cavities were performed using the v^2–f, S–A and two-layer k–ϵ turbulence models. Configurations with various geometrical parameters (rib-to-rib distance, rib height, cavity depth) were considered. Comparison between the predictions and available experimental data confirm that the k–ϵ model severely underpredicts the heat transfer rate. The S–A model gives heat transfer predictions that are closer to the experimental data but the predicted values of *Nu* are still far from the desired values. Of all the numerical simulations carried out in this study, heat transfer predictions by the v^2–f model were closest to the experimental values.

A shortcoming in predictive capability for flow in ribbed channels has been identified. The secondary flow structure observed in the experiments was not present in any of the numerical simulations. This led to incorrect

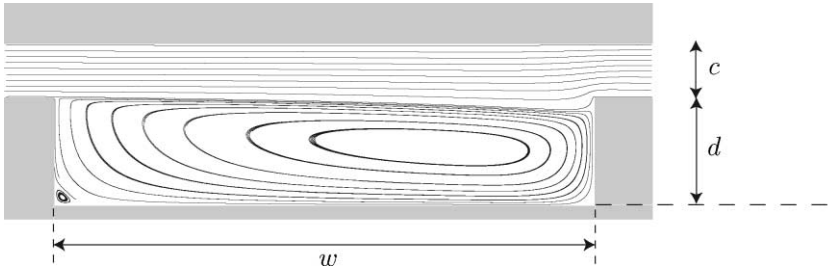

Fig. 10. Streamlines for the blade tip configuration with $c/w = 0.1$ and $d/w = 0.2$ at $Re = 15{,}000$.

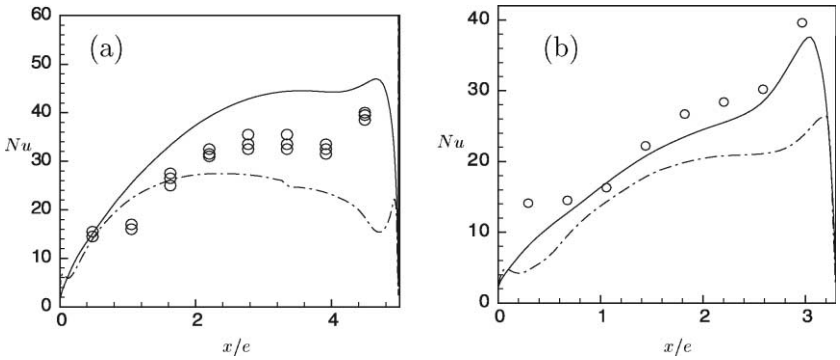

Fig. 11. Nusselt number for the blade tip configuration. $d/w = 0.1$ (a) and $d/w = 0.2$ (b). (◯) Experimental data, (—) v^2–f, (- - - -) k–ϵ. $Re = 15{,}000$, $Pr = 0.71$.

qualitative and quantitative prediction of *Nu* on the side wall.

References

Barth, T.J., Jesperson, D., 1989. The design and application of upwind schemes on unstructured meshes. In: AIAA-89-0366, AIAA 27th Aerospace Sciences Meeting, Reno, Nevada.

Behnia, M., Parneix, S., Durbin, P., 1998. Prediction of heat transfer in an axisymmetric turbulent jet impinging on a flat plate. Int. J. Heat Mass Transfer 41, 1845–1855.

Behnia, M., Parneix, S., Shabany, Y., Durbin, P.A., 1999. Numerical study of turbulent heat transfer in confined and unconfined impinging jets. Int. J. Heat Fluid Flow 20, 1–9.

Bardina, J.E., Huang, P.G., Coakley T.J., 1997. Turbulence modeling validation, testing, and development. NASA TM 110446.

Chen, H.C., Patel, V.C., 1988. Near-wall turbulence models for complex flows including separation. AIAA J. 26 (6), 641–648.

Chyu, M.K., Wu, L.X., 1989. Combined effects of rib angle-of-attack and pitch-to-height ratio on mass transfer from a surface with transverse ribs. Exp. Heat Transfer 2, 291–308.

Durbin, P.A., 1995. Separated flow computations with the k–$\epsilon - v^2$ model. AIAA J. 33, 659–664.

Durbin, P.A., Pettersson-Reif, B.A., 2001. Statistical Theory and Modeling for Turbulent Flows. John Wiley & Sons, New York.

Gatski, T.B., Speziale, C.G., 1993. On explicit algebraic stress models for complex turbulent flows. J. Fluid Mech. 254, 59–78.

Han, J.C., Glicksman, L.R., Rohsenow, W.M., 1978. An investigation of heat transfer and friction for rib-roughened surfaces. Int. J. Heat Mass Transfer 21, 1143–1156.

Han, J.C., Park, J.S., Lei, C.K., 1985. Heat transfer enhancement in channels with turbulence promoters. J. Eng. Gas Turb. Power 107, 628–635.

Hirota, M., Yosokawa, H., Fujita, H., 1992. Turbulence kinetic energy in turbulent flows through square ducts with rib-roughened walls. Int. J. Heat Fluid Flow 13 (1), 22–29.

Iacovides, H., Raisee, M., 1999. Recent progress in the computation of flow and heat transfer in internal cooling passages of turbine blades. Int. J. Heat Fluid Flow 20, 320–328.

Iacovides, H., 1998. Computation of flow and heat transfer through rotating ribbed passages. Int. J. Heat Fluid Flow 19, 393–400.

Kalitzin, G., Iaccarino, G., 1999. Endwall heat transfer computations in a transonic turbine cascade. In: XVII Congresso nazionale sulla transmissione del calore U.I.T, Ferrara, 30 June–2 July.

Kays, W.M., 1994. Turbulent Prandtl number-where are we? J. Heat Transfer 116, 284–295.

Liou, T.M., Hwang, J.J., Chen, S.H., 1993a. Simulation and measurement of enhanced turbulent heat transfer in a channel with periodic ribs on one principal wall. Int. J. Heat Mass Transfer 36 (2), 507–517.

Liou, T.-M., Wu, Y.-Y., Chang, Y., 1993b. LDV measurements of periodic fully developed main and secondary flows in a channel with rib-disturbed walls. J. Fluids Eng. 115, 109–114.

Metzger, D.E., Bunker, R.S., Chyu, R.K., 1989. Cavity heat transfer on a transverse grooved wall in a narrow flow channel. J. Heat Transfer 111, 73–79.

Parneix, S., Durbin, P.A., Behnia, M., 1998. Computation of 3-D turbulent boundary layers using the V2F model. Flow, Turbulence Combust. 60, 19–46.

Rau, G., Cakan, M., Moeller, D., Arts, T., 1998. The effect of periodic ribs on the local aerodynamic and heat transfer performance of a straight cooling channel. J. Turbomach. 120, 368–375.

Simoneau, R.J., Simon, F.F., 1992. Progress towards understanding and predicting heat transfer in the turbine gas path. Int. J. Heat Fluid Flow 14 (2), 106–128.

Speziale, C., 1997. Comparison of explicit and traditional algebraic stress models of turbulence. AIAA J. 35 (9), 1506–1509.

Stephens, M.A., 1995. Computation of flow and heat transfer in a rectangular channel with ribs. AIAA Paper 95-0180.

Spalart, P.R., Allmaras, S.R., 1992. A one-equation turbulence model for aerodynamic flows. AIAA 92-0439.

Webb, R.L., Eckert, E.R.G., Goldstein, R.J., 1971. Heat transfer and friction in tubes with repeated-rib roughness. Int. J. Heat Mass Transfer 14, 601–617.